Human Molecular Genetics, 2020, Vol. 29, No. 15 2461–2470

doi: 10.1093/hmg/ddaa102
Advance Access Publication Date: 29 May 2020
General Article

GENERAL ARTICLE

Pharmacological read-through of R294X Mecp2 in a novel mouse model of Rett syndrome

Jonathan K. Merritt[1,2,3], Bridget E. Collins[4,5], Kirsty R. Erickson[2,3], Hongwei Dong[2,3] and Jeffrey L. Neul[1,2,3,*]

[1]Department of Neurosciences, University of California at San Diego, La Jolla, CA 92093, USA, [2]Department of Pediatrics, Vanderbilt University Medical Center, Nashville, TN 37212, USA, [3]Vanderbilt Kennedy Center, Vanderbilt University Medical Center, Nashville, TN 37203, USA, [4]Medical Scientist Training Program, Vanderbilt University, Nashville, TN 37232, USA and [5]Vanderbilt Brain Institute, Vanderbilt University, Nashville, TN 37232, USA

*To whom correspondence should be addressed at: Vanderbilt Kennedy Center, 405 One Magnolia Circle Bldg., 110 Magnolia Circle, Nashville, TN 37203, USA. Tel: +1 (615) 3228242; Fax: +1 (615) 3228236; Email: jeffrey.l.neul@vumc.org

Abstract

Rett syndrome (RTT) is a neurodevelopmental disorder primarily caused by mutations in *Methyl-CpG-binding Protein 2* (*MECP2*). More than 35% of affected individuals have nonsense mutations in *MECP2*. For these individuals, nonsense suppression has been suggested as a possible therapeutic approach. To assess the viability of this strategy, we created and characterized a mouse model with the common p.R294X mutation introduced into the endogenous *Mecp2* locus (*Mecp2*^{R294X}). *Mecp2*^{R294X} mice exhibit phenotypic abnormalities similar to those seen in complete null mouse models; however, these occur at a later time point consistent with the reduced phenotypic severity seen in affected individuals containing this specific mutation. The delayed onset of severe phenotypes is likely due to the presence of truncated MeCP2 in *Mecp2*^{R294X} mice. Supplying the *MECP2* transgene in *Mecp2*^{R294X} mice rescued phenotypic abnormalities including early death and demonstrated that the presence of truncated MeCP2 in these mice does not interfere with wild-type MeCP2. In *vitro* treatment of a cell line derived from *Mecp2*^{R294X} mice with the nonsense suppression agent G418 resulted in full-length MeCP2 protein production, demonstrating feasibility of this therapeutic approach. Intraperitoneal administration of G418 in *Mecp2*^{R294X} mice was sufficient to elicit full-length MeCP2 protein expression in peripheral tissues. Finally, intracranial ventricular injection of G418 in *Mecp2*^{R294X} mice induced expression of full-length MeCP2 protein in the mouse brain. These experiments demonstrate that translational read-through drugs are able to suppress the *Mecp2* p.R294X mutation *in vivo* and provide a proof of concept for future preclinical studies of nonsense suppression agents in RTT.

Introduction

Rett syndrome (RTT, OMIM #312750) is a severe neurodevelopmental disorder primarily caused by mutations in the X-linked transcriptional regulator *Methyl-CpG-Binding Protein 2* (*MECP2*) (1). Affected individuals experience relatively normal initial development, but then undergo regression between 18 and 30 months of life (2) with loss of acquired spoken language and purposeful hand use and development of characteristic hand stereotypies and gait abnormalities (3). People with RTT also develop a

Received: March 31, 2020. **Revised:** May 21, 2020. **Accepted:** May 27, 2020

variety of additional clinical features including movement abnormalities, seizures, breathing dysfunction and cardiac rhythm abnormalities (1,4–6). While over 200 RTT causing mutations have been identified in *MECP2*, ∼70% of patients have one of eight recurrent mutations (p.R106W, p.R133C, p.T158M, p.R168X, p.R255X, p.R270X, p.R294X and p.R306C) (7,8). Currently, there is no intervention that significantly alters the disease course, and treatment remains at a symptomatic basis, although recent early-stage clinical trials show some promise for new therapeutic approaches (9,10). Studies in mouse models of RTT have shown that postnatal activation of functional MeCP2 rescues many disease phenotypes, providing hope that increasing functional MeCP2 levels could be a viable therapeutic strategy (11–14).

More than 35% of RTT individuals have nonsense mutations in *MECP2* (nmRTT) (7,8). For these people, pharmacological suppression of premature termination codons in *MECP2* could be a novel therapeutic approach to MeCP2 protein expression. First observed as a feature of aminoglycosides such as gentamicin, 'read-through' compounds allow for translational bypass of premature termination codons and production of full-length protein from nonsense transcripts (15). However, at therapeutic doses, canonical aminoglycosides result in ototoxicity and nephrotoxicity (16). To circumvent these off-target effects, eukaryotic ribosomal selective glycosides, e.g. NB54, NB84 and ELX-02, have been engineered with reduced toxicity and increased read-through efficiency (17,18). Alternatively, non-glycoside small molecule read-through agents, e.g. PTC124/Ataluren/Translarna, have been developed (19). Demonstrated efficacy of these compounds in rodent models of numerous genetic disorders arising from nonsense mutations has spurred widespread interest in their clinical application (20–22). Currently, ELX-02 is in phase II clinical trials for cystinosis (NCT04069260) and cystic fibrosis (NCT04135495). Ataluren/Translarna has conditional authorization status from the European Medicines Agency for the treatment of Duchenne Muscular Dystrophy, and clinical trials against numerous other disorders are underway. Whether these therapeutics will show efficacy for RTT is a topic of current inquiry. While studies in patient-derived cells have shown that treatment with read-through compounds is sufficient to elicit full-length MeCP2 from nonsense transcripts, *in vivo* evidence of molecular or therapeutic efficacy is lacking (23).

The limited number of nmRTT animal models has hindered preclinical development of nonsense suppression therapy for RTT. Mouse models of the common p.R168X and p.R255X mutations have been created and recapitulate many phenotypes of *MECP2* dysfunction (24,25). Although molecular efficacy of read-through compound treatment has been demonstrated in cultured fibroblasts from these mice, *in vivo* efficacy has not been reported. Extended chronic dose studies in these models are complicated by reduced longevity in male p.R168X (median survival 57 days) and p.R255X (median survival 61 days) mice (24,25). Likewise, other severe phenotypes observed in these mice may mask therapeutic effect in preclinical drug screens (24,25). Access to a nmRTT mouse model with reduced phenotypic severity and increased longevity would greatly benefit the development of nonsense suppression as a viable therapeutic. Clinical observation has shown that while p.R168X and p.R255X are associated with increased disease severity, individuals with the common p.R294X mutation have milder clinical features (7,8). Moreover, cellular studies have shown that nonsense suppression is more efficient in the context of p.R294X compared to other *MECP2* mutations (25,26). Combined, these findings suggest that an animal model of the p.R294X mutation might be ideal to test nonsense suppression therapies in RTT.

To complement existing mouse models of nmRTT, we generated a new mouse model carrying a recurrent *MECP2* nonsense mutation, p.R294X (*Mecp2*^{R294X}). Validating their utility as a preclinical model of RTT, *Mecp2*$^{R294X/Y}$ mice display phenotypes associated with MeCP2 dysfunction. However, *Mecp2*$^{R294X/Y}$ mice have dramatically increased longevity and a protracted progression of severe phenotypes compared to existing nmRTT models. Molecular characterization revealed that the reduced severity observed in these mice is associated with the stable expression of a truncated MeCP2 protein in the context of p.R294X, which is not observed in the previously characterized nonsense mutations in *MECP2*. Despite having a milder phenotype compared to existing nmRTT models, *Mecp2*$^{R294X/Y}$ mice mimic motor, learning and breathing abnormalities clinically associated with RTT. We characterized these behavioral and physiological phenotypes to provide metrics for assessing therapeutic effect in future drug studies. To assess the utility of *Mecp2*$^{R294X/Y}$ mouse for preclinical studies of nonsense suppression therapeutics, we determined the efficacy of the prototypic read-through compound G418 *in vitro* and *in vivo*. We found that full-length MeCP2 protein could be expressed in *Mecp2*$^{R294X/Y}$ ear-tip fibroblasts and *Mecp2*$^{R294X/Y}$ mice treated with G418. These findings establish the *Mecp2*^{R294X} mouse as a valid model of RTT and provide a basis for conducting preclinical studies of nonsense suppression therapeutic efficacy in this model.

Results

Mecp2$^{R294X/Y}$ mice exhibit milder phenotypes compared to other models of nmRTT and express a stable truncated MeCP2 protein.

Using CRISPR–Cas9-directed mutagenesis, we generated a mouse line with R294X precisely knocked into the endogenous *Mecp2* locus (Fig. 1A) (27). Of 70 mutagenized embryos, allele-specific polymerase chain reaction (PCR) identified 23 mice with the expected knock-in. To ensure scarless insertion of p.R294X, we sequenced the coding regions of *Mecp2* and established three lines from founders that showed sequence integrity across all exons outside of the desired p.R294X mutation. Hemizygous males from all three lines showed similar severity and survival phenotypes (Supplementary Material, Fig. S1). A single engineered mouse was selected and backcrossed to C57BL/6J for eight generations to ensure consistency of the background and to eliminate possible other off-target mutations prior to characterization. As with other models of MeCP2 dysfunction, *Mecp2*$^{R294X/Y}$ mice show a progressive increase in phenotypic severity (Fig. 1B) and decreased longevity (Fig. 1C) compared with wild-type mice (WT). However, *Mecp2*$^{R294X/Y}$ mice show a delayed onset of severe phenotypes (Fig. 1B) and increased longevity (Fig. 1C) compared with the previously reported *Mecp2*$^{R255X/Y}$ mouse model (24). Improvements in survival and phenotypic severity in *Mecp2*$^{R294X/Y}$ mice are also apparent when compared with the findings from a report characterizing a *Mecp2*$^{R168X/Y}$ mouse model (25). Because an absence of truncated MeCP2 protein was reported in both the *Mecp2*$^{R168X/Y}$ and *Mecp2*$^{R255X/Y}$ mice (24,25), we asked if the milder phenotype of *Mecp2*$^{R294X/Y}$ mice is caused by the presence of truncated protein. Immunoblotting mouse brain lysates with an antibody against the MeCP2 amino-terminus revealed a truncation product at the predicted size of 45 kDa

in samples from *Mecp2*$^{R294X/Y}$ mice (Fig. 1D). Notably, a highly sensitive biotin–streptavidin signal amplification system failed to detect truncated MeCP2 in samples from Mecp2$^{R255X/Y}$ mice (Fig. 1D). Immunofluorescence staining of mouse cortex showed strong nuclear-localized N-terminal MeCP2 signal in WT and *Mecp2*$^{R294X/Y}$ samples, while no signal was apparent in *Mecp2*$^{R255X/Y}$ samples (Fig. 1E). Probing with an antibody specific to the MeCP2 C-terminus did not yield detectable signal in samples from either mutant mouse indicating a lack of full-length protein (Fig. 1E). Together, these findings suggest that the mild phenotype observed in *Mecp2*$^{R294X/Y}$ mice is associated with expression of truncated MeCP2 protein.

R294X-truncated MeCP2 co-localization with heterochromatic foci (Fig. 1E) suggests that DNA binding activity is preserved in the truncated protein. To interrogate the nature of this interaction, we purified nuclei from mouse brains for differential NaCl fractionation of DNA-bound proteins (Fig. 1F). Surprisingly, R294X-truncated MeCP2 protein demonstrated an increased affinity for DNA as shown by decreased elution at 300 mM NaCl compared to WT (Fig. 1G). These results suggest that while DNA binding is preserved in R294X-truncated MeCP2, the affinity of this interaction is altered compared to the WT protein.

The presence of a nuclear-localized truncation product with increased affinity for DNA could disrupt functional MeCP2 rescue. To evaluate this possibility, we asked if full-length MeCP2 complementation could improve gross phenotypes in *Mecp2*$^{R294X/Y}$ mice. Introducing transgenic *MECP2* (28) in R294X mice (*Mecp2*$^{R294X/Y}$; *MECP2*^{Tg1}) was sufficient to rescue these phenotypes, and no significant difference in severity (Fig. 1H) or survival (Fig. 1I) was seen compared to WT mice. Similarly, transgenic *MECP2* was sufficient to rescue an underweight phenotype observed in *Mecp2*$^{R294X/Y}$ mice (Supplementary Material, Fig. S2). While nuclear-localized truncated MeCP2 is present in R294X mice, the phenotypic rescue by full-length MeCP2 demonstrated here indicates the mutant protein does not significantly interfere with full-length MeCP2 function. Thus, *Mecp2*$^{R294X/Y}$ mice are a viable model for assessing therapeutics centered upon restoring functional MeCP2 activity.

Mecp2$^{R294X/Y}$ mice display motor dysfunction and deficits in learning and memory

To establish the R294X mouse as a preclinical model, we asked if behavior abnormalities typified in other models of MeCP2 dysfunction were present in *Mecp2*$^{R294X/Y}$ mice. We conducted a behavior battery in 16-week-old mice because phenotypic severity increases at this time (Fig. 1B). *Mecp2*$^{R294X/Y}$ mice had impaired motor function and decreased motor learning when evaluated using the accelerating rotating rod task (rotarod) (Fig. 2A). Similarly, *Mecp2*$^{R294X/Y}$ mice showed impaired motor dysfunction on the forepaw wire hanging task, with mutant animals falling sooner off the wire compared to WT control animals (Fig. 2B). *Mecp2*$^{R294X/Y}$ mice were hypoactive with decreased distance traveled in the open field arena (Fig. 2C). Consistent with other mouse models of MeCP2 dysfunction, *Mecp2*$^{R294X/Y}$ mice had an increased preference for the center zone of the arena, suggesting that this mutation promotes reduced anxiety compared to WT (Fig. 2C). Deficits in hippocampal- and amygdala-dependent learning were also apparent in *Mecp2*$^{R294X/Y}$ mice as shown by decreased freezing compared to WT in contextual and cued fear conditioning tasks (Fig. 2D) (29,30). *Mecp2*$^{R294X/Y}$ mice also displayed abnormal gait patterns characterized by decreased hind paw stride length and decreased longitudinal deviation (Fig. 2E). Despite *Mecp2*$^{R294X/Y}$ mice having a milder phenotype

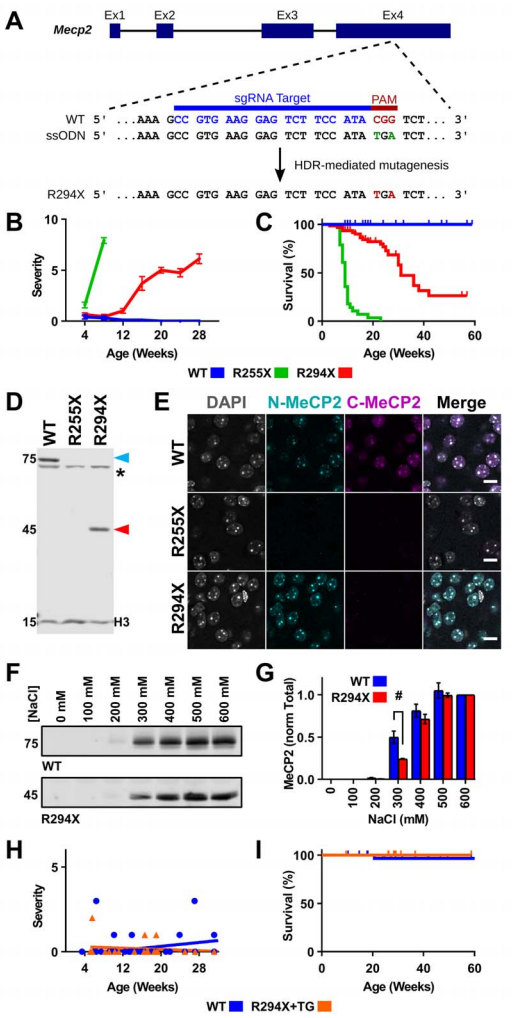

Figure 1. *Mecp2*$^{R294X/Y}$ mice have a mild phenotype compared to *Mecp2*$^{R255X/Y}$ mice due to the presence of truncated MeCP2 protein. (**A**) A schematic representation of the CRISPR–Cas9-directed mutagenesis approach to introduce R294X into the endogenous *Mecp2* locus. (**B**) *Mecp2*$^{R294X/Y}$ mice (red line, $n = 10$) display progression of MeCP2 dysfunction phenotypes (Severity, Bird Scoring) at a slower rate compared to *Mecp2*$^{R255X/Y}$ mice (green line, $n = 13$), while severe phenotypes are not observed in WT mice (blue line, $n = 11$). (**C**) *Mecp2*$^{R294X/Y}$ mice (red line, $n = 61$) have an early death phenotype compared to WT (blue line, $n = 39$) but greater longevity compared to *Mecp2*$^{R255X/Y}$ mice (green line, $n = 28$). (**D**) Western blotting of whole brain lysates with an antibody against the amino terminus of MeCP2 shows that truncated protein is present in *Mecp2*$^{R294X/Y}$ mice, but not *Mecp2*$^{R255X/Y}$ mice. Full-length MeCP2 (75 kDa) is absent in samples from either mutant mouse. Blue arrow: full-length MeCP2; asterisk: nonspecific band; red arrow: truncated MeCP2; H3: histone H3 loading control. (**E**) Immunofluorescence staining of mouse cortex with antibodies specific to either the amino or carboxy terminus of MeCP2 confirms the presence of nuclear-localized truncation product in *Mecp2*$^{R294X/Y}$ mice, but not *Mecp2*$^{R255X/Y}$ mice. Scale bar = 10 μm. (**F**, **G**) R294X-truncated MeCP2 retains DNA binding function. Differential salt fractionation of purified nuclei from *Mecp2*$^{R294X/Y}$ mouse brain shows that truncated MeCP2 (red bars, $n = 3$) has increased affinity for DNA compared to WT protein (blue bars, $n = 3$) by reduced elution of the truncated protein at 300 mM NaCl. (F) A representative western blot of NaCl extracted nuclei and (G) quantification of biological replicates ($n = 3$ per genotype) normalized to Ponceau S staining and presented as a fraction of full-length or truncated MeCP2 extracted at 600 mM (Total). $^{\#}P < 0.001$, differences calculated by *t*-tests with Holm–Sidak correction for multiple comparisons. Error bars are standard error of the mean (SEM). (**H**) Linear regression of scattershot severity phenotyping from *Mecp2*$^{R294X/Y}$,*MECP2*^{Tg1} mice (orange line, $n = 18$) and WT mice (blue line, $n = 34$). *Mecp2*$^{R294X/Y}$,*MECP2*^{Tg1} mice do not exhibit severe phenotypes. (**I**) *Mecp2*$^{R294X/Y}$,*MECP2*^{Tg1} mice (orange line, $n = 18$) show similar longevity to WT mice (blue line, $n = 34$).

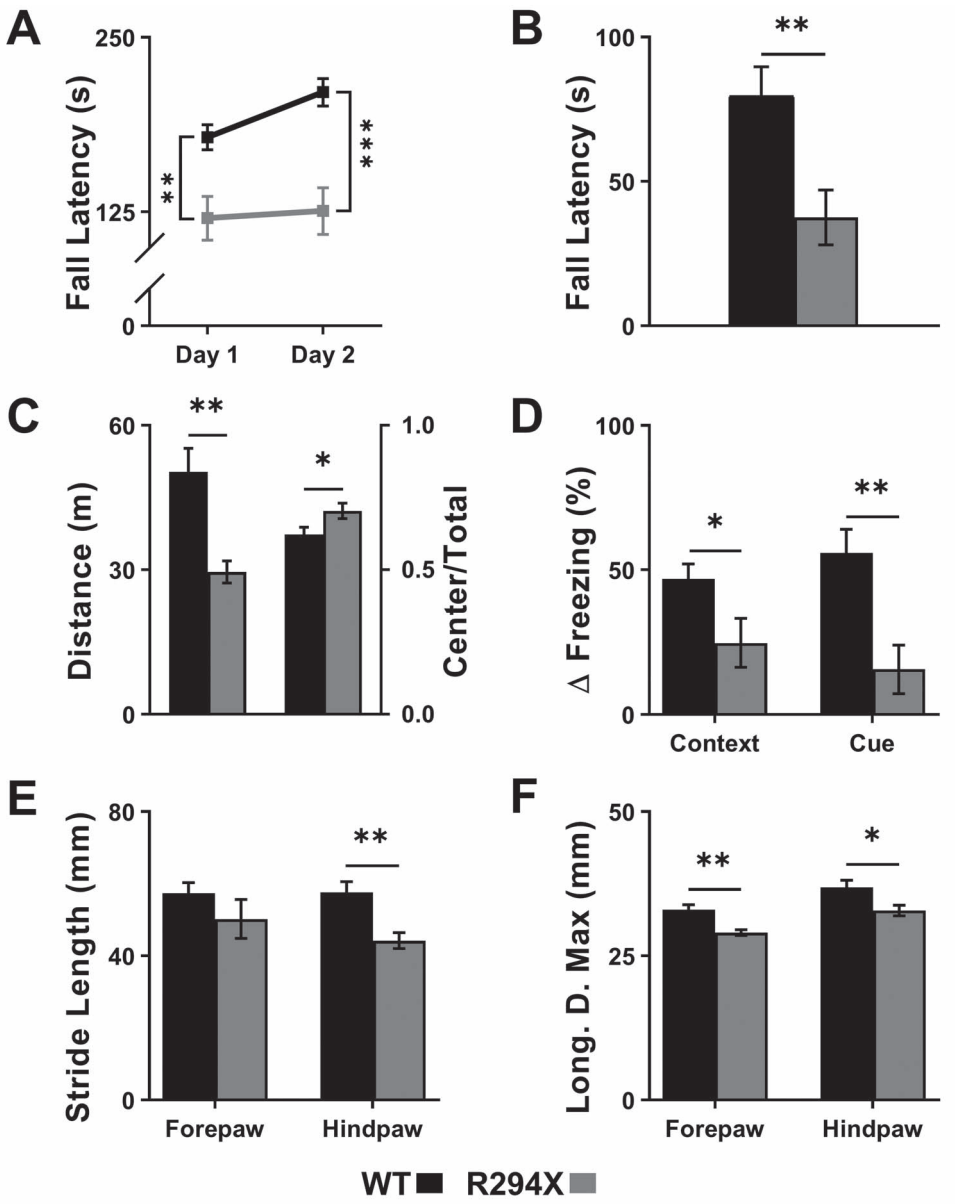

Figure 2. R294X mice have abnormal motor and learning phenotypes at 16 weeks of age. (**A**) *Mecp2*$^{R294X/Y}$ mice (grey points, $n = 9$) show impaired performance on and are unable to learn an accelerating rotor rod task compared to WT (black points, $n = 11$). (**B**) These mice also perform poorly on a forepaw wire hang assay. (**C**) *Mecp2*$^{R294X/Y}$ mice are hypoactive and show increased preference for the center of the arena on an open field assay. (**D**) Context and cued freeze responses are reduced in *Mecp2*$^{R294X/Y}$ mice ($n = 8$) compared to WT ($n = 10$) following fear conditioning. (**E**, **F**) *Mecp2*$^{R294X/Y}$ mice ($n = 7$) have an abnormal gait compared to WT ($n = 9$) characterized by altered stride length (E) and longitudinal deviation (Long.D.Max) (F). $^{***}P < 0.001$, $^{**}P < 0.01$, $^{*}P < 0.05$ differences calculated by a t-test. Error bars are SEM.

compared to other RTT models, these findings indicate that R294X-truncated MeCP2 is not sufficient to prevent motor and learning dysfunctions.

Mecp2$^{R294X/Y}$ mice have abnormal breathing and atypical electroencephalography activity

Because RTT patients and existing models of MeCP2 dysfunction have breathing irregularities and abnormal cortical electroencephalography (EEG) activity, we asked if similar traits were present in *Mecp2*$^{R294X/Y}$ mice. Unrestrained whole-body plethysmography revealed that *Mecp2*$^{R294X/Y}$ mice have breathing dysfunction (Fig. 3A). Specifically, *Mecp2*$^{R294X/Y}$ mice have an increased breathing rate (Fig. 3B), increased breathing irregularity (Fig. 3C) and an elevated incidence of apneas compared to WT (Fig. 3D). The salient breathing phenotype in *Mecp2*$^{R294X/Y}$ mice provides a defined physiological outcome measure for future preclinical studies in this model.

During routine handling, a subset of Mecp2$^{R294X/Y}$ mice was observed to have absence seizure-like events. While seizures were not detected in 9-week-old Mecp2$^{R294X/Y}$ mice, free moving video-coupled EEG recordings repeated at 13 weeks of age revealed spontaneous seizure activity, which was not present in WT litter mates (Fig. 3E). In one Mecp2$^{R294X/Y}$ mouse, three seizure-like episodes scored as 1–2 on a modified Racine scale (31) with increased digging and head nodding were captured over a 24-h period. In a second Mecp2$^{R294X/Y}$ mouse, two seizures persisting for more than 60 s and scored as 4 on the Racine scale

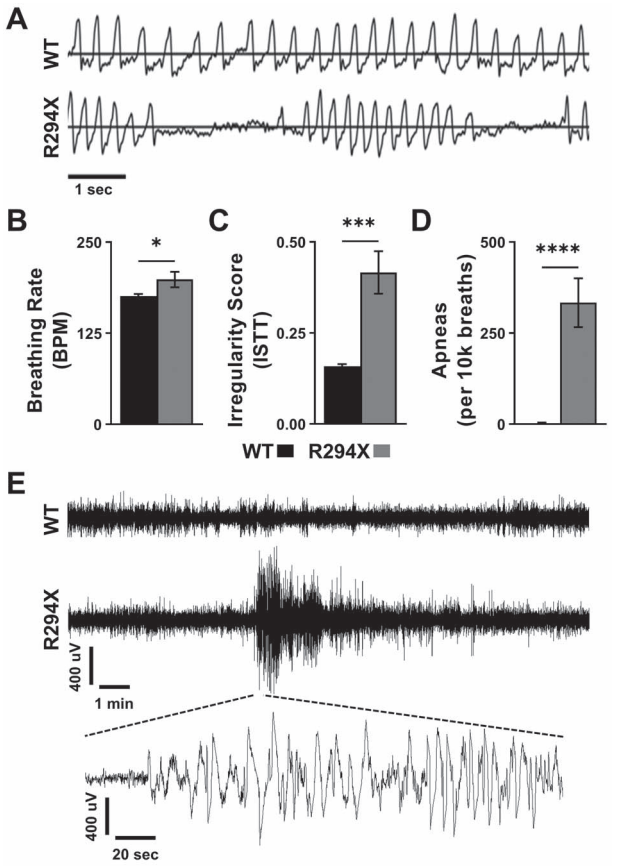

Figure 3. R294X mice have breathing abnormalities and seizure-like cortical activity. (**A**) *Mecp2*$^{R294X/Y}$ mice have an altered breathing pattern compared to WT mice at 16 weeks of age. (**B**) The basal breathing rate in *Mecp2*$^{R294X/Y}$ mice (grey bars, $n = 9$) is elevated compared to WT (black bars, $n = 11$). BPM, breaths per minute. (**C**) *Mecp2*$^{R294X/Y}$ mice have an elevated breathing irregularity score compared to WT. ISTT, instantaneous rate of change in total breath time. (**D**) Apnea events are greatly increased in *Mecp2*$^{R294X/Y}$ mice compared to WT. (**E**) Representative filtered (0.5–50 Hz bandpass) EEG traces from a period of normal awake activity in a 13-week-old WT mouse (top) and a period of awake activity disrupted by a seizure in a 13-week-old *Mecp*$^{R294X/Y}$ mouse (bottom). The expanded view shows baseline immediately prior to onset of a seizure and chaotic, high voltage discharges present during the seizure. $^{****}P < 0.0001$, $^{***}P < 0.001$, $^{**}P < 0.01$, $^{*}P < 0.05$ differences calculated by a *t*-test. Error bars are SEM.

with characteristic tonic body contractions and rearing were observed during the 24-h recording (Supplementary Material, Video). Though further study is needed to fully characterize this apparent seizure phenotype, the findings reported here suggest that seizures manifest in Mecp2$^{R294X/Y}$ mice in accordance with the phenotypic severity progression observed between 9 and 13 weeks of age (Fig. 1B).

Read-through compound treatment suppresses R294X and allows full-length MeCP2 production in murine adult fibroblasts

A key question is whether read-through compounds are able to effectively allow the production of full-length MeCP2 protein from the R294X containing transcript. To aid in rapid scalable screening of candidate read-through therapeutics, we generated immortalized adult ear tip fibroblasts (iETFs) from *Mecp2*$^{R294X/Y}$ and *Mecp2*$^{R255X/Y}$ mice. When treated with the prototypic read-through compound G418, but not vehicle, both mutant iETFs (R255X or R294X) produced full-length Mecp2 protein (Fig. 4A); however, nonsense mutation read-through was more robust in *Mecp2*$^{R294X/Y}$ iETFs across all doses with a notable 2-fold increase in full-length protein at 200 µg/ml G418 compared to *Mecp2*$^{R255X/Y}$ (Fig. 4B). A defined dose escalation response was observed in *Mecp2*$^{R294X/Y}$ iETFs with increased G418 concentration yielding greater full-length MeCP2 production (Fig. 4B), but no significant difference in full-length MeCP2 level was seen between G418 concentrations in *Mecp2*$^{R255X/Y}$ iETFs (Fig. 4B). These findings suggest that read-through of nonsense *Mecp2* transcripts is more efficient in the context of *Mecp2*$^{R294X/Y}$. This is in accordance with previous studies in patient-derived cells and exogenous constructs that showed the R294X allele was more efficiently suppressed than other common nonsense mutations in *MECP2* (25,26). Combined, these results suggest that nonsense suppression agents may show greater therapeutic effect in the R294X mouse, indicating this model as an ideal platform for *in vivo* screening of read-through compound efficacy.

Read-through compound treatment is sufficient to restore full-length MeCP2 in *Mecp2*$^{R294X/Y}$ mice *in vivo*

Despite numerous publications demonstrating small-molecule suppression of *MECP2* nonsense mutations *in vitro*, a similar demonstration of efficacy *in vivo* has not been reported. Because aminoglycosides, like G418, are not expected to cross the blood–brain barrier (BBB) in therapeutically relevant quantities, we asked if intraperitoneal (IP) injection of G418 was sufficient to restore full-length MeCP2 protein in peripheral tissue targets. G418 administered at 30 mg/kg IP for 14 days was sufficient to promote detectable levels of full-length MeCP2 protein in the lungs of *Mecp2*$^{R294X/Y}$ mice, but not saline-treated controls (Fig. 5A and B). To circumvent BBB penetration issues, we used intracranial ventricular (ICV) injection of G418 to assess suppression of the R294X mutation in the mouse brain. Two ICV infusions of 80 µg G418 over 4 days resulted in full-length MeCP2 expression in treated *Mecp2*$^{R294X/Y}$ mice, but not saline controls (Fig. 5C), providing proof of concept that this class of drugs allows read-through in the brain and production of full-length MeCP2 protein from the *Mecp2*^{R294X} allele. While full-length MeCP2 protein could be resolved by western blotting, the quantity of drug-induced protein was insufficient to yield robust detection by immunofluorescence staining in sectioned brain tissue from treated mice (data not shown). The difference in full-length MeCP2 detected in treated mice (Fig. 5C) is likely due to inconsistencies in cannulation and infusion between mice as shown by more complete ventricular staining with trypan blue post euthanasia in the mouse showing a greater full-length protein level (Supplementary Material, Fig. S3).

Discussion

A key step in the development of viable nonsense suppression therapy in RTT requires preclinical evaluation in cell and animal models that have high construct and face validity of the human disease. Here, we created and characterized a new mouse model of RTT arising from the common R294X mutation. This model has high construct validity because it represents a human mutation knocked into the exogenous locus, as opposed to exogenous constructs based on cDNA expression systems. Furthermore, these mutant mice recapitulate many phenotypes of the human disorder, thus showing high face validity, and are well suited for application to future preclinical studies and drug development. Moreover, the increased longevity and comparatively slow progression of phenotypic severity in *Mecp2*$^{R294X/Y}$ mice make

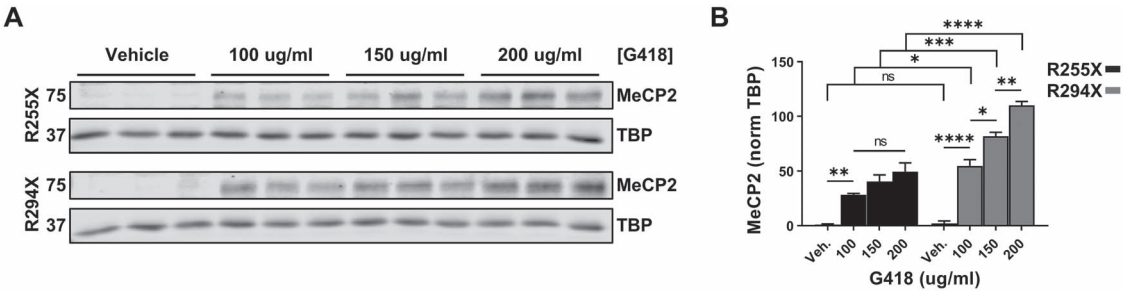

Figure 4. Read-through compound treatment promotes full-length MeCP2 expression in fibroblasts from *Mecp2*$^{R294X/Y}$ mice. (**A**) Representative western blot of *Mecp2*$^{R255X/Y}$ and *Mecp2*$^{R294X/Y}$ immortalized ear tip fibroblasts treated with vehicle, 100, 150 or 200 μg/ml G418 for 48 h. G418 treatment restores full-length MeCP2 protein expression, while no full-length protein is detected in vehicle-treated cells. Each lane corresponds to an individual treatment experiment. (**B**) Quantification of three experimental replicates of G418 treatment reveals that the R294X allele (grey bars) is more efficiently suppressed than the R255X allele (black bars) across all interrogated doses. ****$P < 0.0001$, ***$P < 0.001$, **$P < 0.01$, *$P < 0.05$ with differences in full-length MeCP2 between genotype and G418 dose calculated by a two-way analysis of variance with Tukey's *post hoc* for multiple comparisons. Error bars are SEM.

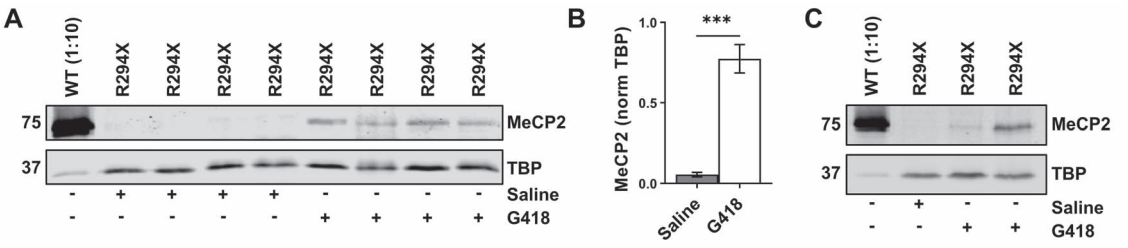

Figure 5. Read-through compound treatments promote MeCP2 expression in *Mecp2*$^{R294X/Y}$ mice *in vivo*. (**A**) Representative western blot of lung lysates from *Mecp2*$^{R294X/Y}$ mice treated with 30 mg/kg G418 delivered by IP injection for 14 days and saline controls. Each lane corresponds to an individually treated mouse. (**B**) Quantification shows that full-length MeCP2 is detected in the lungs of G418-treated mice (white bar, $n = 4$), but not saline controls (grey bar, $n = 4$). (**C**) Representative western blot of brain lysates from *Mecp2*$^{R294X/Y}$ mice dosed with either 80 μg G418 ($n = 2$) or saline ($n = 1$) by ICV injection twice over a 4-day period. Full-length MeCP2 is present in the brains of treated mice, while no full-length protein is detected in saline-treated mice. ***$P < 0.001$ differences calculated by a *t*-test. Error bars are SEM.

them a useful addition to the collection of existing RTT models for pathogenesis studies. Finally, we developed immortalized cell lines from this mouse line that can provide the basis for expanded screening of compounds that are effective at read-through from the exogenous *Mecp2* locus.

Surprisingly, truncated MeCP2 protein was detected in the *Mecp2*^{R294X} mouse brain. Previous studies of *Mecp2*^{R168X} and *Mecp2*^{R255X} mice did not identify truncated MeCP2 protein in the context of either mutation (24,25). Furthermore, truncated MeCP2 protein was not detected in human brain lysates from patients with R168X, R255X or R270X mutation (24). Of the common RTT-causing nonsense mutations, it appears that truncated MeCP2 production is unique to the R294X allele. The mechanism allowing for truncated MeCP2 in the context of R294X, but not other common nonsense mutations, is a focus of ongoing investigation. The presence of truncated MeCP2 likely explains the less severe phenotype observed in *Mecp2*^{R294X} mice in this study. Similarly, the presence of truncated MeCP2 may underlie the reduced clinical severity associated with RTT patients who have a R294X mutation (7,8). Because R294X MeCP2 retains DNA-interacting functions, neomorphic or dominant negative effects of this truncated protein could interfere with gene therapy and pharmacological strategies aimed at restoring functional MeCP2 expression. In this study, transgenic MeCP2 supplied in conjunction with the R294X allele rescued gross phenotypes observed in mutant animals, suggesting that full-length MeCP2 is able to interact with its targets and execute normal functions. However, these methods are not sufficient to elucidate if an overexpression-like phenotype, similar to MeCP2 duplication syndrome (28,32,33), results from providing functional MeCP2 in the context of R294X MeCP2. Understanding the intersectional effects of R294X truncated and full-length MeCP2 will be critical for determining the viability of therapeutics aimed at fully restoring functional MeCP2 levels.

Beyond characterizing this new mouse model, we demonstrated the utility of the R294X mouse in assessing nonsense suppression therapy efficacy. Importantly, we found that MeCP2 nonsense mutations can be pharmacologically suppressed *in vivo*. A key unanswered question is if the quantity of read-through-induced full-length MeCP2 is sufficient to rescue disease phenotypes in the R294X mouse. Currently available read-through compounds have been shown to restore 20–30% of normal full-length MeCP2 levels in cellular assays (25). Further chronic treatment studies are needed to determine if similar levels of full-length MeCP2 can be achieved with nonsense suppression *in vivo* in the R294X mouse. While G418 treatment in this study restored full-length MeCP2 protein in the brain and peripheral tissue, it is unclear if the limited quantity of full-length MeCP2 detected would modify disease phenotypes. The molecular efficacy demonstrated here provides a rational basis for conducting the large-scale trials necessary for assessing therapeutic efficacy. However, the chronic dose-associated toxicity of canonical aminoglycosides precludes the use of compounds like G418 in long-term studies. PTC124 or lead Eloxx compounds, e.g. ELX-02, are well suited for such studies due to their reduced toxicity profiles and improved pharmacokinetics (18,19). Indeed, studies in a mouse model of Hurler syndrome suggest that PTC124 crosses the BBB (34), while Eloxx is currently pursuing targeted delivery strategies for their lead compounds that will improve BBB permeability (35). In future studies, the *Mecp2*^{R294X} mouse and immortalized cellular

models reported here will be a valuable resource for developing these read-through compounds and other therapeutics as viable interventions for RTT.

Materials and Methods

Mice

All methods and procedures were approved either by the University of California San Diego or Vanderbilt University Medical Center Animal Care and Use Program, and mice were housed in AALAC-approved facilities. *Mecp2*$^{R294X/Y}$ mice were derived through pronuclear injection of 0.5 days post fertilization C57BL/6 embryos with *in vitro* transcribed sgRNA targeting p.R294 in *Mecp2*, a ssODN repair template encoding p.R294X with 50 bp homology arms on either side of the mutation, and Cas9 mRNA. Mosaic pups were screened for successful mutagenesis by restriction enzyme-mediated genotyping for a unique *Nde*I site formed by p.R294X, and by allele-specific PCR. Following sequencing of the *Mecp2* coding regions, three founder lines were established, which had sequence integrity across all coding exons except for the desired p.R294X mutation. Gross phenotyping showed no difference between offspring of these founder lines, and a single line was backcrossed to WT C57BL/6J mice for eight generations prior to characterization. *Mecp2*$^{R255X/Y}$ and *MECP2*^{TG1} mice were maintained as previously described (24).

Immunoblotting for MeCP2

Mice were humanely euthanized and perfused with PBS prior to dissection of specified tissues. Nuclear protein lysates were obtained by homogenizing tissue in 10 mM Hepes, 1.5 mM $MgCl_2$, 10 mM KCl, 0.05% NP40, 0.5 mM DTT and 1× Mammalian Protease Inhibitor Cocktail (Sigma, St. Louis, MO USA, P8340), pH 7.9. Following centrifugation to remove the cytosolic fraction, nuclei were suspended in 5 mM Hepes, 1.5 mM $MgCl_2$, 0.2 mM EDTA, 0.5 mM DTT, 1× Mammalian Protease Inhibitor Cocktail and 25% glycerol, pH 7.9. Suspended nuclei were sonicated prior to a 1-h incubation with Benzonase (Sigma E1014). Following nuclease treatment, NaCl concentration was raised to 300 mM, and samples were incubated for 30 min prior to high-speed centrifugation to remove debris. Protein concentration was quantified with 660 nm Protein Assay Reagent (Pierce, Waltham, MA USA), and 30 µg protein per lane was loaded onto house-made 7.5 or 10% acrylamide SDS-PAGE gels and subjected to standard western blotting procedures. An Odyssey CLx (LI-COR, Lincoln, Nebraska USA) imaging system was used for western blot detection, and quantification was performed in Image Studio (LI-COR). Full-length MeCP2 was detected with an antibody specific to the last 19 amino acids of MeCP2 (Cell Signaling, Danvers, MA USA, D4F3; 1:1000 dilution). Truncated MeCP2 was detected with an antibody specific to exon 3 (Sigma Men-8; 1:500 dilution). As a loading control, mouse anti-TBP was used (Abcam ab51841, 1:2000). Secondary antibodies used for detection were goat anti-rabbit 800CW (LI-COR 926–32 211; 1:10000) and goat anti-mouse 680RD (LI-COR 926–68 070; 1:10000). For increased sensitivity in experiments probing truncation product in *Mecp2*$^{R255X/Y}$ mice, a biotinylated goat anti-mouse secondary antibody was used (Jackson ImmunoResearch, West Grove, PA USA, #115–065-068; 1:5000) followed by a tertiary incubation with Alexa Fluor 680-conjugated streptavidin (Invitrogen, Carlsbad, CA USA, S32358; 1:5000).

NaCl fractionation of nuclear proteins

NaCl fractionation was performed on nuclei isolated as described above. Following suspension in 5 mM Hepes, 1.5 mM $MgCl_2$, 0.2 mM EDTA, 0.5 mM DTT, 1× Mammalian Protease Inhibitor Cocktail, 25% glycerol, pH 7.9, equivalent volumes of nuclei were split across seven 1.5 ml tubes, and NaCl concentration was adjusted to 0, 100, 200, 300, 400, 500 or 600 mM in an equivalent volume of buffer. Following a 1-h incubation, samples were centrifuged at high speed, and supernatants were immunoblotted for MeCP2 amino terminus as described above. Quantified MeCP2 levels were normalized to Ponceau S staining and recorded as the fraction of MeCP2 extracted with 600 mM NaCl (Total MeCP2).

Immunohistochemistry

Mice were humanely euthanized and perfused with PBS/4% PFA prior to dissection of whole brains. Following an overnight post-fixation in PBS/4% PFA, tissue was cryoprotected in 30% Sucrose/PBS, mounted in optimal cutting temperature compound, and 40 µm thick cryosections were collected. Heat-induced epitope retrieval (HIER) was essential for achieving robust Men-8 detection of the MeCP2 amino-terminus. HIER was performed by transferring sections to 10 mM trisodium citrate, 0.05% Tween-20 pH 6.0 and heating to 80°C for 30 min. Following equilibration in PBS, floating sections were permeabilized in 0.3% TritonX-100/PBS and blocked in 10% Normal Donkey Serum, 0.3% TritonX-100/PBS. After blocking, sections were incubated with the following primary antibodies overnight at 4°C: mouse anti-MeCP2 amino terminus (Sigma Men-8; 1:250 dilution) and chicken anti-MeCP2 full-length (Millipore, Burlington, MA USA, Abe171; 1:500 dilution). Sections were then washed in 0.3% TritonX-100/PBS and incubated with the following secondary antibodies for 4 h at room temperature: Alexa Fluor 488-conjugated donkey anti-mouse IgG (Jackson ImmunoResearch #715–545-150; 1:500 dilution) and Alexa Fluor 594-conjugated donkey anti-chicken IgY (Jackson ImmunoResearch #703–545-155; 1:500 dilution). Nuclei were counterstained with DAPI (0.1 µg/ml in PBS) and mounted in ProLong Gold Antifade reagent. 63× images of the cortex were collected using a Zeiss LSM 710 confocal microscope available through the Vanderbilt Cell Imaging Shared Resource. Exposure settings were defined using a WT sample and held constant for imaging R255X and R294X mutant samples. Image processing was performed in ImageJ.

Mouse characterization

Mouse behavior and physiology experiments were all performed at the Vanderbilt University Neurobehavioral Core Facility. Observers were blinded to the mouse genotype for all assays. Severity phenotyping was performed based on Bird Scoring (12) where mice are given a score of '0' (no phenotype), '1' (phenotype present) or '2' (severe phenotype) for general appearance, hind limb clasping, activity, tremor, breathing abnormalities, hunched back and gait. Gait analysis was performed using a Cleversys TreadScan (Reston, VA USA) forced gait apparatus (31). For assessment of motor function, a wire hang assay was performed where mice were placed on a suspended wire such that only their forelimbs were in contact, and the latency to fall was recorded across a 2-min trial (36). Accelerating rotating rod (rotarod) assessment of motor learning was performed using a two-day paradigm. Briefly, on Day 1, mice were placed on a rotarod apparatus (Ugo Basile, Gemonio, Italy) with an acceleration from 0 to 40 rpm over 5 min, and latency to fall was recorded for four repeated 5-min trials. After 24 h (Day 2), the rotarod paradigm was repeated. Weight and survival metrics were calculated as previously described (37).

Conditioned fear

The conditioned fear paradigm consisted of a training day where mice were allowed to freely explore a test chamber (square walls and a wire floor with white light) for 2 min before a 30-s tone was played paired with a 0.5 mA foot shock in the final 2 s of the tone stimulus. Following a 2-min consolidation period, the tone–shock sequence was repeated, and mice were allowed to recover within the chamber for 1 min before being returned to their home cage. The following morning, contextual memory was assayed by returning mice to the test chambers for 4 min while freezing events were recorded. After 2 h, mice were placed in novel chambers consisting of rounded walls, a flat floor, no light and vanilla aroma. Following 2 min of free exploration in the novel chamber, cued memory was assayed by playing the tone stimulus from the training day for 2 min while freezing events were recorded. The change in freezing response from training to trial day (ΔFreezing) was calculated for each animal by subtracting the training day pre-stimulus percent freezing from the trial percent freezing. Differences between genotypes were calculated with a *t*-test.

Whole body plethysmography

Whole body plethysmography data were captured as previously described (5). A custom Python script was used to analyze breathing data from calm segments where minimal physical activity was detected in time-locked video recordings. Breathing irregularity (instantaneous rate of change in total breath time) was calculated as the instantaneous change in breath duration between adjacent breaths. Apneas were defined for breaths with >0.5 s duration as pauses lasting more than two times the local and overall average breath duration. Apneas were reported as the number of pauses meeting these criteria per 10 000 breaths.

In vivo EEG

Mice were implanted with a two-channel EEG/one-channel EMG headmount (Pinnacle, Lawrence, KS USA) at 8 weeks of age. Following 7 days of recovery, 24-h EEG recordings were captured with time-locked video monitoring at 9 weeks of age. The 24-h recordings were repeated at 13 weeks of age. Seizure-like events were scored by a blinded reviewer from recorded videos using a modified Racine scale (31) and confirmed by inspection of EEG traces filtered with a second-order Butterworth bandpass from 0.5 to 50 Hz.

Cell culture

Adult ear tip fibroblasts were cultured from 2 mm ear punches collected as part of standard mouse tagging. In an approach similar to previously described methods, collected tissue was cleaned with ethanol, minced and individual tissue pieces were transferred to a thin film of media in a 35 mm dish for fibroblast outgrowth (38). Culture media for fibroblast outgrowth and maintenance consisted of DMEM (Gibco, Carlsbad, CA USA, 11 995–065), 10% FBS (GeminiBio, West Sacramento, CA), 1× Mem-NEAA (Gibco) and 1× Pen-strep (Gibco). Approximately 2 weeks after fibroblast outgrowth, cells were passaged with 0.05% Trypsin (Gibco) and immortalized by calcium phosphate transfection of pBSSVD2005 encoding the SV40 large T antigen (Addgene plasmid #21826). Transfected cells were serial passaged at a 1:10 split to enrich transformed cells as described previously (39). G418 treatment was performed by dissolving drug directly in media at the specified concentrations. Following 48 h of treatment, nuclear protein lysates were prepared and western blotting for full-length MeCP2 was performed as described above.

IP and ICV G418 injection

Intraperitoneal injection studies were conducted by dissolving G418 in sterile saline to a stock concentration of 5 mg/ml. Daily injections yielding 30 mg/kg G418 were given for 14 days prior to euthanasia and isolation of specified tissues as described above. For ICV delivery of G418, mice were surgically implanted with a cannula in the right lateral ventricle. Briefly, standard aseptic surgical techniques were followed to implant a cannula (P1 Technologies, Roanoke, VA) at A/P +0.46 mm, M/L +1.00 mm, D/V −2.7 mm to bregma. Following a 1-week recovery period, mice were infused at a rate of 0.4 µl/min with 0.8 µl saline as a control or 0.8 µl of 100 mg/ml G418 in sterile saline (Day 1), a dose previously reported as sufficient to suppress nonsense mutations in the adult mouse brain (40). Infusions were repeated on Day 3, and mice were euthanized for tissue collection on Day 5. Following euthanasia, 5 µl of Trypan blue was rapidly flushed through the cannula to confirm proper placement by complete staining of the ventricular system. Nuclear protein lysates were prepared as described above from an ∼18 mm^3 block of tissue dissected about the right lateral ventricle. Western blotting for full-length MeCP2 was performed as described above.

Statistical analysis

All data plots were created, and statistical analyses were performed with Prism 8 (GraphPad, San Diego, CA USA). All bar graphs show the mean ± standard error of the mean. Scatterplots of severity scores for *Mecp2*$^{WT/Y}$, *Mecp2*$^{R255X/Y}$ and *Mecp2*$^{R294X/Y}$ mice (Fig. 1B) show averaged scores within genotypes at each time point connected by a fitted curve. Scatterplots of severity scores for founder lines 1, 2 and 3 of *Mecp2*$^{R294X/Y}$ mice (Supplementary Material, Fig. S1B) show scores for individual mice at each time point with plotted lines showing within founder line linear regression across all time points. Scatterplots of severity scores for *Mecp2*$^{WT/Y}$ and *Mecp2*$^{R294X/Y}$,*MECP2*^{Tg1} mice (Fig. 1H) show scores for individual mice at each time point with plotted lines showing within genotype linear regression across all time points. Scatterplots of weights for *Mecp2*$^{WT/Y}$, *Mecp2*$^{R294X/Y}$ and *Mecp2*$^{R294X/Y}$,*MECP2*^{Tg1} mice (Supplementary Material, Fig. S2) show weights for individual mice at each time point with plotted lines showing within genotype two-knot spline regression across all time points. Differences in efficiency of MeCP2 elution at different NaCl concentrations between genotypes were calculated using *t*-tests with Holm–Sidak correction for multiple comparisons. Comparisons of quantitative behavior and physiological data (Figs 2 and 3) between genotypes were performed using a *t*-test. Comparisons between genotype and G418 dose in drug-treated fibroblast experiments (Fig. 4) were determined by a two-way analysis of variance with Tukey's *post hoc* for multiple comparisons.

Supplementary Material

Supplementary Material is available at *HMG* online.

Funding

RettSyndrome.org (#2906 and #3201 to J.L.N.); U.S. National Institutes of Health (grants HD083181 and U54HD083211 to

J.L.N.); National Institutes of Health (grants CA68485, DK20593, DK58404, DK59637 and EY08126).

Acknowledgements

The content is solely the responsibility of the authors and does not necessarily represent the official views of the National Institutes of Health or the Eunice Kennedy Shriver Child Health and Human Development Institute (NICHD). Rodent experiments were performed in part through the use of the Murine Neurobehavior Core lab at the Vanderbilt University Medical Center. Imaging experiments were performed in part through the use of the Vanderbilt Cell Imaging Shared Resource. We thank the UCSD Moores Cancer Center Transgenic Mouse Shared Resource for assistance with CRISPR pronuclear injection.

Conflict of Interest Statement: The authors have no conflicts to report.

References

1. Amir, R.E., Van den Veyver, I.B., Wan, M., Tran, C.Q., Francke, U. and Zoghbi, H.Y. (1999) Rett syndrome is caused by mutations in X-linked MECP2, encoding methyl-CpG-binding protein 2. *Nat. Genet.*, **23**, 185–188.
2. Neul, J.L., Glaze, D.G., Percy, A.K., Feyma, T., Beisang, A., Dinh, T., Suter, B., Anagnostou, E., Snape, M., Horrigan, J. *et al.* (2015) Improving treatment trial outcomes for Rett syndrome: the development of Rett-specific anchors for the clinical global impression scale. *J. Child Neurol.*, **30**, 1743–1748.
3. Neul, J.L., Kaufmann, W.E., Glaze, D.G., Christodoulou, J., Clarke, A.J., Bahi-Buisson, N., Leonard, H., Bailey, M.E.S., Schanen, N.C., Zappella, M. *et al.* (2010) Rett syndrome: revised diagnostic criteria and nomenclature. *Ann. Neurol.*, **68**, 944–950.
4. FitzGerald, P.M., Jankovic, J. and Percy, A.K. (1990) Rett syndrome and associated movement disorders. *Mov. Disord.*, **5**, 195–202.
5. Guideri, F., Acampa, M., DiPerri, T., Zappella, M. and Hayek, Y. (2001) Progressive cardiac dysautonomia observed in patients affected by classic Rett syndrome and not in the preserved speech variant. *J. Child Neurol.*, **16**, 370–373.
6. Tarquinio, D.C., Hou, W., Neul, J.L., Berkmen, G.K., Drummond, J., Aronoff, E., Harris, J., Lane, J.B., Kaufmann, W.E., Motil, K.J. *et al.* (2018) The course of awake breathing disturbances across the lifespan in Rett syndrome. *Brain Dev.*, **40**, 515–529.
7. Neul, J.L., Fang, P., Barrish, J., Lane, J., Caeg, E.B., Smith, E.O., Zoghbi, H., Percy, A. and Glaze, D.G. (2008) Specific mutations in methyl-CpG-binding protein 2 confer different severity in Rett syndrome. *Neurology*, **70**, 1313–1321.
8. Cuddapah, V.A., Pillai, R.B., Shekar, K.V., Lane, J.B., Motil, K.J., Skinner, S.A., Tarquinio, D.C., Glaze, D.G., McGwin, G., Kaufmann, W.E. *et al.* (2014) Methyl-CpG-binding protein 2 (MECP2) mutation type is associated with disease severity in Rett syndrome. *J. Med. Genet.*, **51**, 152–158.
9. Glaze, D.G., Neul, J.L., Percy, A., Feyma, T., Beisang, A., Yaroshinsky, A., Stoms, G., Zuchero, D., Horrigan, J., Glass, L. *et al.* (2017) A double-blind, randomized, placebo-controlled clinical study of Trofinetide in the treatment of Rett syndrome. *Pediatr. Neurol.*, **76**, 37–46.
10. Glaze, D.G., Neul, J.L., Kaufmann, W.E., Berry-Kravis, E., Condon, S., Stoms, G., Oosterholt, S., Della Pasqua, O., Glass, L., Jones, N.E. *et al.* (2019) Double-blind, randomized, placebo-controlled study of trofinetide in pediatric Rett syndrome. *Neurology*, **92**, e1912–e1925.
11. Gadalla, K.K., Bailey, M.E., Spike, R.C., Ross, P.D., Woodard, K.T., Kalburgi, S.N., Bachaboina, L., Deng, J.V., West, A.E., Samulski, R.J. *et al.* (2013) Improved survival and reduced phenotypic severity following AAV9/MECP2 gene transfer to neonatal and juvenile male Mecp2 knockout mice. *Mol. Ther.*, **21**, 18–30.
12. Guy, J., Gan, J., Selfridge, J., Cobb, S. and Bird, A. (2007) Reversal of neurological defects in a mouse model of Rett syndrome. *Science*, **315**, 1143–1147.
13. Garg, S.K., Lioy, D.T., Cheval, H., McGann, J.C., Bissonnette, J.M., Murtha, M.J., Foust, K.D., Kaspar, B.K., Bird, A. and Mandel, G. (2013) Systemic delivery of MeCP2 rescues behavioral and cellular deficits in female mouse models of Rett syndrome. *J. Neurosci.*, **33**, 13612–13620.
14. Giacometti, E., Luikenhuis, S., Beard, C. and Jaenisch, R. (2007) Partial rescue of MeCP2 deficiency by postnatal activation of MeCP2. *Proc. Natl. Acad. Sci.*, **104**, 1931–1936.
15. Dabrowski, M., Bukowy-Bieryllo, Z. and Zietkiewicz, E. (2015) Translational readthrough potential of natural termination codons in eucaryotes – the impact of RNA sequence. *RNA Biol.*, **12**, 950–958.
16. Lacy, M.K., Nicolau, D.P., Nightingale, C.H. and Quintiliani, R. (1998) The pharmacodynamics of aminoglycosides. *Clin. Infect. Dis.*, **27**, 23–27.
17. Pokrovskaya, V., Nudelman, I., Kandasamy, J. and Baasov, T. (2010) Chapter twenty-one—Aminoglycosides: redesign strategies for improved antibiotics and compounds for treatment of human genetic diseases. In Fukuda, M. (ed), *Methods in Enzymology, Glycomics*. Academic Press, Cambridge MA, USA, Vol. **478**, pp. 437–462.
18. Nudelman, I., Rebibo-Sabbah, A., Cherniavsky, M., Belakhov, V., Hainrichson, M., Chen, F., Schacht, J., Pilch, D.S., Ben-Yosef, T. and Baasov, T. (2009) Development of novel aminoglycoside (NB54) with reduced toxicity and enhanced suppression of disease-causing premature stop mutations. *J. Med. Chem.*, **52**, 2836–2845.
19. Welch, E.M., Barton, E.R., Zhuo, J., Tomizawa, Y., Friesen, W.J., Trifillis, P., Paushkin, S., Patel, M., Trotta, C.R., Hwang, S. *et al.* (2007) PTC124 targets genetic disorders caused by nonsense mutations. *Nature*, **447**, 87–91.
20. Gregory-Evans, C.Y., Wang, X., Wasan, K.M., Zhao, J., Metcalfe, A.L. and Gregory-Evans, K. (2014) Postnatal manipulation of Pax6 dosage reverses congenital tissue malformation defects. *J. Clin. Invest.*, **124**, 111–116.
21. Keeling, K.M., Wang, D., Dai, Y., Murugesan, S., Chenna, B., Clark, J., Belakhov, V., Kandasamy, J., Velu, S.E., Baasov, T. *et al.* (2013) Attenuation of nonsense-mediated mRNA decay enhances in vivo nonsense suppression. *PLoS One*, **8**, e60478.
22. Xue, X., Mutyam, V., Tang, L., Biswas, S., Du, M., Jackson, L.A., Dai, Y., Belakhov, V., Shalev, M., Chen, F. *et al.* (2014) Synthetic aminoglycosides efficiently suppress cystic fibrosis transmembrane conductance regulator nonsense mutations and are enhanced by Ivacaftor. *Am. J. Respir. Cell Mol. Biol.*, **50**, 805–816.
23. Vecsler, M., Ben Zeev, B., Nudelman, I., Anikster, Y., Simon, A.J., Amariglio, N., Rechavi, G., Baasov, T. and Gak, E. (2011) Ex vivo treatment with a novel synthetic aminoglycoside NB54 in primary fibroblasts from Rett syndrome patients suppresses MECP2 nonsense mutations. *PLoS One*, **6**, e20733.

24. Pitcher, M.R., Herrera, J.A., Buffington, S.A., Kochukov, M.Y., Merritt, J.K., Fisher, A.R., Schanen, N.C., Costa-Mattioli, M. and Neul, J.L. (2015) Rett syndrome like phenotypes in the R255X Mecp2 mutant mouse are rescued by MECP2 transgene. *Hum. Mol. Genet.*, **24**, 2662–2672.
25. Brendel, C., Belakhov, V., Werner, H., Wegener, E., Gärtner, J., Nudelman, I., Baasov, T. and Huppke, P. (2011) Readthrough of nonsense mutations in Rett syndrome: evaluation of novel aminoglycosides and generation of a new mouse model. *J. Mol. Med.*, **89**, 389–398.
26. Popescu, A.C., Sidorova, E., Zhang, G. and Eubanks, J.H. (2010) Aminoglycoside-mediated partial suppression of MECP2 nonsense mutations responsible for Rett syndrome in vitro. *J. Neurosci. Res.*, **88**, 2316–2324.
27. Cong, L., Ran, F.A., Cox, D., Lin, S., Barretto, R., Habib, N., Hsu, P.D., Wu, X., Jiang, W., Marraffini, L.A. *et al.* (2013) Multiplex genome engineering using CRISPR/Cas systems. *Science*, **339**, 819–823.
28. Collins, A.L., Levenson, J.M., Vilaythong, A.P., Richman, R., Armstrong, D.L., Noebels, J.L., David Sweatt, J. and Zoghbi, H.Y. (2004) Mild overexpression of MeCP2 causes a progressive neurological disorder in mice. *Hum. Mol. Genet.*, **13**, 2679–2689.
29. Kim, J.J. and Fanselow, M.S. (1992) Modality-specific retrograde amnesia of fear. *Science*, **256**, 675–677.
30. Phillips, R.G. and LeDoux, J.E. (1992) Differential contribution of amygdala and hippocampus to cued and contextual fear conditioning. *Behav. Neurosci.*, **106**, 274–285.
31. Gogliotti, R.G., Senter, R.K., Rook, J.M., Ghoshal, A., Zamorano, R., Malosh, C., Stauffer, S.R., Bridges, T.M., Bartolome, J.M., Daniels, J.S. *et al.* (2016) mGlu5 positive allosteric modulation normalizes synaptic plasticity defects and motor phenotypes in a mouse model of Rett syndrome. *Hum. Mol. Genet.*, **25**, 1990–2004.
32. Samaco, R.C., Mandel-Brehm, C., McGraw, C.M., Shaw, C.A., McGill, B.E. and Zoghbi, H.Y. (2012) Crh and Oprm1 mediate anxiety-related behavior and social approach in a mouse model of MECP2 duplication syndrome. *Nat. Genet.*, **44**, 206–211.
33. Ramocki, M.B., Peters, S.U., Tavyev, Y.J., Zhang, F., Carvalho, C.M.B., Schaaf, C.P., Richman, R., Fang, P., Glaze, D.G., Lupski, J.R. *et al.* (2009) Autism and other neuropsychiatric symptoms are prevalent in individuals with MeCP2 duplication syndrome. *Ann. Neurol.*, **66**, 771–782.
34. Bedwell, D.M., Wang, D., Welch, E.M. and Keeling, K.M. (2015) The nonsense suppression drug PTC124 restored alpha-l-iduronidase activity and reduces glycosaminoglycan accumulation in MPS IH mice carrying the Idua-W402X mutation. *Mol. Genet. Metab.*, **114**, S20.
35. Eloxx Pharmaceuticals, Inc. (2017) 2017 Form 10-K. https://investors.eloxxpharma.com/static-files/c8705a19-c0fc-4d4e-846a-713d412f48c9 (accessed Feb 18, 2020).
36. Samaco, R.C., Fryer, J.D., Ren, J., Fyffe, S., Chao, H.-T., Sun, Y., Greer, J.J., Zoghbi, H.Y. and Neul, J.L. (2008) A partial loss of function allele of methyl-CpG-binding protein 2 predicts a human neurodevelopmental syndrome. *Hum. Mol. Genet.*, **17**, 1718–1727.
37. Ward, C.S., Arvide, E.M., Huang, T.-W., Yoo, J., Noebels, J.L. and Neul, J.L. (2011) MeCP2 is critical within HoxB1-derived tissues of mice for normal lifespan. *J. Neurosci.*, **31**, 10359–10370.
38. Vangipuram, M., Ting, D., Kim, S., Diaz, R. and Schüle, B. (2013) Skin punch biopsy explant culture for derivation of primary human fibroblasts. *J Vis. Exp.* **77**, e3779. doi: 10.3791/3779.
39. Harding, H.P., Zhang, Y., Scheuner, D., Chen, J.-J., Kaufman, R.J. and Ron, D. (2009) Ppp1r15 gene knockout reveals an essential role for translation initiation factor 2 alpha (eIF2α) dephosphorylation in mammalian development. *Proc. Natl. Acad. Sci.*, **106**, 1832–1837.
40. Meng, F., Han, Y., Srisai, D., Belakhov, V., Farias, M., Xu, Y., Palmiter, R.D., Baasov, T. and Wu, Q. (2016) New inducible genetic method reveals critical roles of GABA in the control of feeding and metabolism. *Proc. Natl. Acad. Sci.*, **113**, 3645–3650.